Temporal Airy–Talbot effect in linear optical potentials

Tianwen Han (韩天文)[1], Hao Chen (陈 浩)[1], Wenwan Li (李文纨)[1], Bing Wang (王 兵)[1*], and Peixiang Lu (陆培祥)[1,2]

[1] Wuhan National Laboratory for Optoelectronics and School of Physics, Huazhong University of Science and Technology, Wuhan, 430074, China

[2] Hubei Key Laboratory of Optical Information and Pattern Recognition, Wuhan Institute of Technology, Wuhan 430205, China

*Corresponding author: wangbing@hust.edu.cn

We investigate the Airy–Talbot effect of an Airy pulse train in time-dependent linear potentials. The parabolic trajectory of self-imaging depends on both the dispersion sign and the linear potential gradient. By imposing linear phase modulations on the pulse train, the Airy–Talbot effects accompanied with positive and negative refractions are realized. For an input composed of stationary Airy pulses, the self-imaging follows straight lines, and the Airy–Talbot distance can be engineered by varying the linear potential gradient. The effect is also achieved in symmetric linear potentials. The study provides opportunities to control the self-imaging of aperiodic optical fields in time dimension.

Keywords: Airy pulse; Talbot and self-imaging effect; dispersion; linear potential.
DOI: 10.3788/COL202119.082601

1. Introduction

The Talbot effect refers to the self-imaging phenomenon of a periodic paraxial optical field that was first, to the best of our knowledge, discovered by Talbot in 1836[1]. The effect has been extensively investigated ranging from classical optics and nonlinear optics to quantum optics[2]. The applications have also been widely explored, including optical testing, imaging processing, and photolithography[2]. Since the spatial paraxial diffraction can be analogous to temporal group-velocity dispersion (GVD) in terms of space–time duality[3], the temporal Talbot effect can also be obtained by injecting a periodic optical pulse train into a dispersive medium[4]. In the above Talbot effects, the transverse periodicity of the incident field is required, and self-imaging follows a straight line along the propagation direction[5,6].

Recently, the Airy–Talbot effect was theoretically proposed and experimentally demonstrated in the spatial domain[6–8]. Unlike the traditional Talbot effect, here, the incident field is formed by the superposition of a series of transversely displaced self-accelerating Airy beams[9,10]. The initial intensity pattern reproduces itself periodically along parabolic trajectories in free space. The self-imaging period is termed as Airy–Talbot distance. In addition, the fractional self-images with reduced repetition periods[2] cannot be obtained in the Airy–Talbot scenario. The intrinsic acceleration of the Airy beam can be modified by using external static and dynamic linear potentials, realized by tailoring the transverse and longitudinal refractive index distribution of the medium[11–20]. It is proved that the Airy–Talbot effect in dynamic linear potentials can follow any predefined trajectories by engineering the index gradient,

while the self-imaging distance is the same as that in free space[21–23].

Given the space–time duality, the temporal Airy pulse has also been proposed and demonstrated[9,10,24,25], which possesses intriguing features of non-dispersion and self-acceleration. Differing from the curved propagation trajectory of Airy beams in space, the self-acceleration of Airy pulses leads to varying group velocity during propagation[26]. Analogously, the temporal Airy–Talbot effect can be observed when an Airy pulse train propagates in an optical fiber with GVD[27]. The Airy pulse train can be formed by imposing a cubic spectral phase on the Gaussian pulse train via either third-order dispersion[28,29] or a pulse shaper[30]. The wave train exhibits an accelerating self-imaging phenomenon along parabolic trajectories in the parameter space spanned by propagation distance and time. Compared to the spatial diffraction, the temporal dispersion can be positive or negative, which provides another degree of freedom to control the propagation of the optical pulse. On the other hand, a temporal potential generated by the nonlinear interaction between a weak signal and strong pump lasers[31,32] can be used for either temporal or spectral signal manipulation.

In this work, we investigate the temporal Airy–Talbot effect in time-dependent linear potentials. We show that the accelerating self-imaging process can be enhanced or reduced by applying a linear potential, and the parabolic trajectory of self-imaging depends on both the dispersion sign and the linear potential gradient. By imposing linear phase modulations on the Airy pulse train, we realize the refractive Airy–Talbot effects with positive and negative refractions. For the stationary Airy pulse, having the form of an eigenfunction of the Schrödinger equation for a particle under a uniform force, the self-imaging follows

straight lines, and the Airy–Talbot distance can be controlled by varying the linear potential gradient. The Airy–Talbot effect is also realized in the symmetric linear potential. All of the results can be extended to the spatial Airy beams, corresponding to the anomalous dispersion case here. The study provides a flexible approach to manipulate the Airy–Talbot effect and may find applications in optical communication and signal processing systems based on optical pulses.

2. Theoretical Model

The dynamics of optical pulses in a dispersive medium under a linear potential can be described by[31]

$$i\frac{\partial U}{\partial Z} + \frac{1}{2}k\frac{\partial^2 U}{\partial T^2} + \alpha TU = 0, \tag{1}$$

where $T = (t - z/v_{g0})/t_0$ refers to the normalized retarded time in the frame of reference, which is moving at the initial group velocity of v_{g0}. The real time and propagation distance are denoted by t and z, respectively. t_0 represents the main-lobe width of the Airy pulse. $Z = z/L_{D2}$ is the normalized propagation distance, measured in units of the dispersion length $L_{D2} = t_0^2/|\beta_2|$ with β_2 being the GVD parameter of the medium. $U = As/A_0$ indicates the normalized amplitude of the pulse, where A_s and A_0 are the slowly varying envelope and the input peak amplitude, respectively. $k = 1$ ($k = -1$) denotes the anomalous (normal) GVD. α is the gradient of linear potential. Here, we consider long-duration input pulses, where the impact of higher-order dispersion on pulse propagation is much weaker than that of GVD and hence can be neglected.

3. Results and Discussion

We first study the evolution of a linearly chirped self-accelerating Airy pulse train,

$$U(T,0) = \exp(iCT)\sum_{n\in\mathbb{Z}}c_n\mathrm{Ai}(T - n\Delta)\exp[a(T - n\Delta)], \tag{2}$$

where $\mathrm{Ai}(\cdot)$ represents the Airy function, and c_n is an arbitrary coefficient. Δ is the time interval between the pulses. a is the truncation factor. C denotes the chirp coefficient. Substituting Eq. (2) into Eq. (1), one obtains the corresponding intensity distribution of the propagating solution:

$$I(T,Z) = \left|\sum_{n\in\mathbb{Z}}c_n\mathrm{Ai}\left(T - n\Delta - \frac{Z^2}{4} - kCZ - \frac{k\alpha Z^2}{2} + ikaZ\right)\right.$$
$$\times \exp\left[a(T - n\Delta) - \frac{aZ^2}{2} - \frac{ka\alpha Z^2}{2}\right]$$
$$\times \left.\exp\left(-i\frac{kn\Delta Z}{2}\right)\right|^2. \tag{3}$$

According to Eq. (3), each Airy pulse component has a different phase accumulation rate. Consequently, the initial intensity

profile is reshaped during propagation as a result of interference between the Airy pulses. For ideal Airy pulse trains with $a = 0$, as the propagation distance satisfies the condition $\Delta Z/2 = 2\,m\pi$ with m being a nonzero integer, all of the Airy pulses are in phase. As a result, the input intensity pattern reproduces itself periodically along a modified parabolic trajectory in space–time. As $C = 0$, the trajectory takes the form of $T = Z^2/4 + k\alpha Z^2/2$, which is determined by both the dispersion sign and the gradient of linear potential. In the absence of external potential, i.e., $\alpha = 0$, the self-imaging trajectories in anomalous and normal dispersion regimes are identical. The Airy–Talbot distance is

$$Z_T = \frac{4\pi}{\Delta}. \tag{4}$$

To validate the above analysis, we numerically simulate the evolution of an Airy pulse train under the combined effects of dispersion and time-varying linear potential by using the split-step Fourier method[3]. The input field is composed of seven Airy pulses, separated in time with a constant interval $\Delta = 2$, and each multiplied by $c_n = 1$. According to Eq. (4), we calculate the Airy–Talbot distance of $Z_T = 2\pi$. Figure 1 shows the numerical results of the Airy–Talbot effect for different linear potential gradients in the anomalous dispersion regime. In the case of $\alpha = 0$, the self-imaging follows a parabolic trajectory with the acceleration of $d^2T/dZ^2 = 1/2$ in the T–Z plane, depicted by the white solid curve in Fig. 1(a). The white dashed lines denote the two positions of $Z = 3.14$ and 6.28, at which the self-images are formed. Another place of interest is at half of the Talbot length $z_H = z_T/2$, where there is a π phase
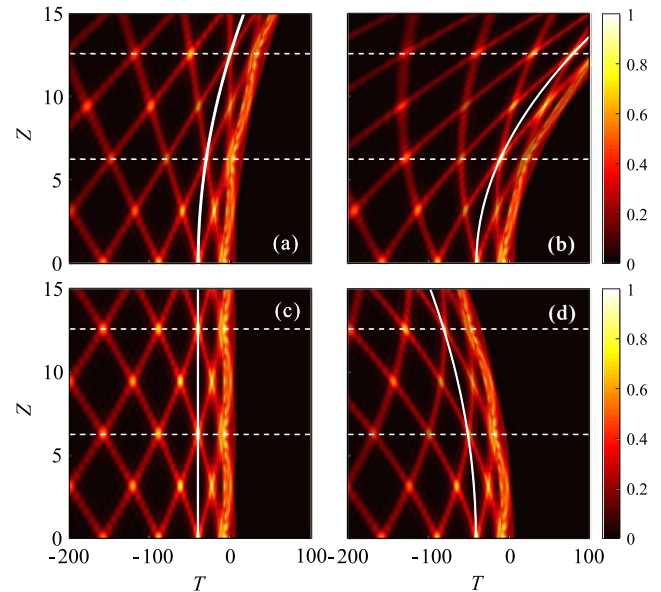

Fig. 1. Airy–Talbot effects for different linear potential gradients of (a) $\alpha = 0$, (b) $\alpha = 1$, (c) $\alpha = -1/2$, and (d) $\alpha = -1$. The white dashed lines indicate the first and second self-imaging positions. The white solid curve denotes the theoretical self-imaging trajectory. Parameters are $a = 0$, $C = 0$, $k = 1$, $\Delta = 2$, $c_n = 1$, and $n \in [3,3]$.

shift between two adjacent Airy pulse components, and the image is phase-shifted relative to the input[21]. The intrinsic acceleration of self-images can be modified by an external force that stems from the linear potential. Figure 1(b) shows the Airy–Talbot carpet for $\alpha = 1$, where the self-imaging is accelerated faster. Interestingly, for $\alpha = -1/2$, the acceleration of self-images can be completely canceled, and the self-imaging is along straight lines, as shown in Fig. 1(c). On the contrary, $\alpha = -1$ will lead to the displacement of self-images in the opposite time dimension, as depicted in Fig. 1(d). In all scenarios, the Airy–Talbot distances are the same as that without linear potential. In the normal dispersion regime, the Airy–Talbot effect exhibits the reversed self-imaging process with respect to that in the anomalous dispersion case and can be analyzed by the same method.

As the input pulse train is modulated by a linearly varying phase, the self-imaging trajectory follows the relation $T = kCZ + Z^2/4 + k\alpha Z^2/2$. The parabolic trajectory of self-images is similar to those of projectiles moving under the action of a uniform gravitational field, and C plays the role of the initial launch velocity. If the intrinsic acceleration is restricted by the external linear potential, the self-imaging follows a straight line with the slope $dT/dZ = kC$. Figure 2(a) shows the Airy–Talbot carpet of a linearly chirped Airy pulse train with $C = 5$, where the other parameters are the same as that in Fig. 1(c). The self-images are linearly shifted along the positive T axis. On the contrary, the linearly chirped Airy pulse train with
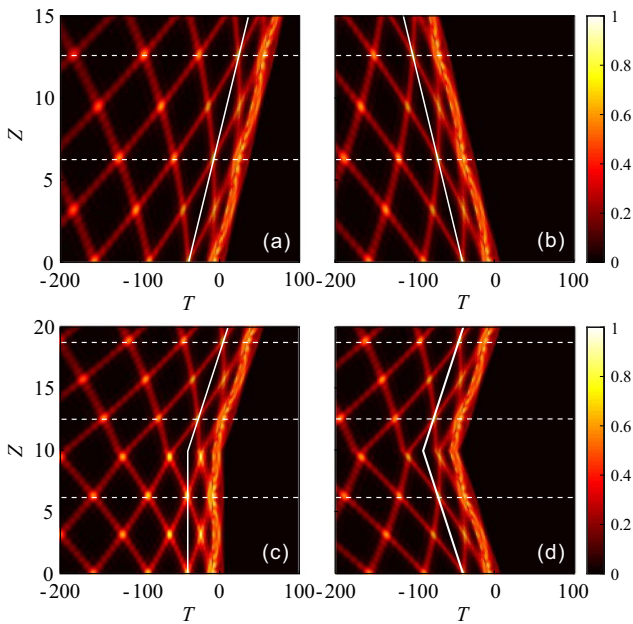
$C = -5$ exhibits a mirror-symmetric evolution with respect to that of $C = 5$, as shown in Fig. 2(b). More interestingly, by imparting another linearly time-varying phase onto the pulse train during propagation, we can realize the refractive Airy–Talbot effect. In Fig. 2(c), the input pulse train is unchirped with $C = 0$ and then modulated by a linearly varying phase with $C = 5$ at $Z = 10$. The white solid line denotes the theoretical self-imaging trajectory, which agrees well with the numerical results. In Fig. 2(d), the pulse train is first linearly modulated by $C = -5$ at $Z = 0$ and then modulated by $C = 10$ at $Z = 10$, leading to an Airy–Talbot effect with negative refraction.

The above analysis indicates that the input field composed of ideal Airy pulses can reproduce itself indefinitely. However, the ideal Airy pulses possess limitless time duration and infinite energy. In practice, we have to truncate the pulses so as to make them have finite energy. According to Eq. (3), the finite-energy Airy pulses (FEAPs) will experience dispersion, and the self-acceleration feature never maintains after the accelerating range, which is comparable to the dispersion length. Here, we choose $a = 0.1$, and the other parameters are the same as in Fig. 1(c). The temporal evolution of the pulse train is shown in Fig. 3(a), where the self-imaging effect disappears. The reason lies in the fact that the Airy–Talbot distance is beyond the accelerating range of FEAPs. In addition, the wave train propagates along a curved trajectory in the T–Z plane when Z is long enough, which is induced by the linear potential. By enlarging the pulse separation to $\Delta = 8$, the self-imaging phenomenon appears, and the Airy–Talbot distance becomes $Z_T = \pi/2$, as shown in Fig. 3(b). For a fixed truncation factor, each Airy pulse has a specific accelerating range and time duration. To decrease the Airy–Talbot distance, we can enlarge the pulse separation
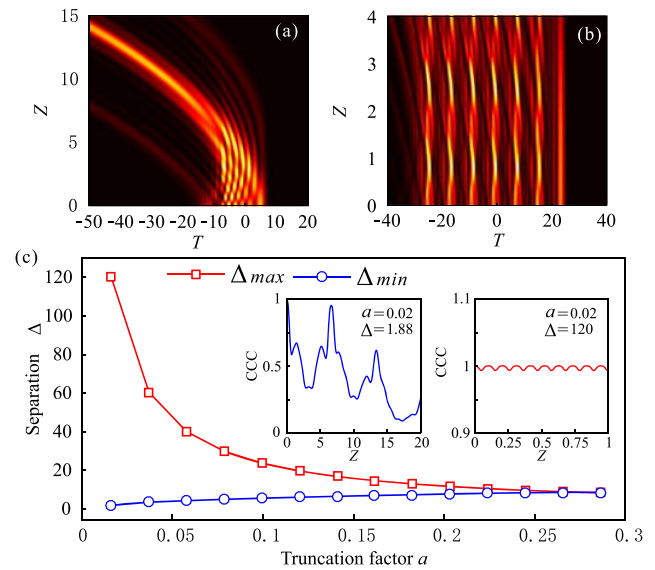

Fig. 2. (a), (b) Airy–Talbot effects of linearly chirped Airy pulse trains with $C = 5$ and $C = -5$, respectively. (c) Refractive Airy–Talbot effect. The input field at $Z = 0$ is unchirped and then linearly chirped with $C = 5$ at $Z = 10$. (d) Negative refractive Airy–Talbot effect. The input field at $Z = 0$ is linearly chirped with $C = -5$ and then chirped with $C = 10$ at $Z = 10$. The white solid line denotes the theoretical self-imaging trajectory. The self-imaging positions are marked by white dashed lines. Other parameters are the same as in Fig. 1(c).

Fig. 3. (a) Temporal evolution of the finite-energy Airy pulse train with $a = 0.1$. Other parameters are the same as in Fig. 1(c). (b) Same as (a) but for $\Delta = 8$. (e) Maximal and minimal pulse separations to realize the Airy–Talbot effect for different truncation factors. The insets show CCC variations versus Z for $\Delta = 1.88$ and 120 in the case of $a = 0.02$.

between the FEAPs. The Airy–Talbot distance corresponding to the minimal pulse separation should be equal to the accelerating range. On the other hand, owing to the Airy–Talbot effect being a result of interference of overlapping Airy pulses, the maximal pulse separation should be less than the time duration of a single pulse. Figure 3(c) shows the numerical results of the allowable maximal and minimal pulse separations to realize the Airy–Talbot effect for different truncation factors. For $a = 0.02$, the maximal and minimal pulse separations are $\Delta_{\max} = 120$ and $\Delta_{\min} = 1.88$, respectively. As a increases, both the time duration and the accelerating range of each pulse decrease. Thus, the maximal pulse separation decreases, and the minimal one increases. As $a > 0.28$, the Airy–Talbot effect cannot be observed. Here, this value is obtained in the framework of a normalized pulse propagation equation. For the practical FEAPs with the main-lobe width t_0, having the form of $\text{Ai}(t/t_0)\exp(at/t_0)$[33], the truncation factor should be a/t_0, which is determined by the main-lobe width of the pulse. To estimate the degree of similarity between the input and the self-images, we use the cross-correlation coefficient (CCC)[4], defined as $\text{CCC} = [\int_{-\infty}^{+\infty} I(T,Z)I(T,0)\mathrm{d}T]/[\int_{-\infty}^{+\infty} I(T,Z)^2\mathrm{d}T]$ $[\int_{-\infty}^{+\infty} I(T,0)^2\mathrm{d}T]^{1/2}$. Here, $I(T, 0)$ is the intensity pattern at $Z = 0$. The value of CCC varies from zero to unity and is equal to unity only if $I(T, Z)$ and $I(T,0)$ are identical. The insets in Fig. 3(e) show CCC evolutions for $\Delta = 1.88$ and 120 when $a = 0.02$. In the former case, the self-image can only be formed at $Z = 6.68$, where the CCC reaches the maximum value. In the latter case, the CCC manifests a periodic variation, confirming the periodic self-imaging effect of the pulse train.

Thus far, we have demonstrated that the parabolic self-imaging trajectory for the Airy–Talbot distance can be modified by the external linear potential. In fact, the stationary eigensolution of Eq. (1) is also an Airy wavefunction. Next, we show that the input field composed of stationary Airy pulses can produce self-images periodically along straight lines. Moreover, the Airy–Talbot distance can be tailored by varying the linear potential gradient. In this case, the input field reads

$$U(T,0) = \sum_{n\in\mathbb{Z}} c_n \text{Ai}[-T_0(T - n\Delta)], \tag{5}$$

where $T_0 = (2\alpha/k)^{1/3}$. The corresponding intensity pattern of the propagating solution is given by

$$I(T,Z) = \left| \sum_{n\in\mathbb{Z}} c_n \text{Ai}[-T_0(T - n\Delta)]\exp(in\alpha\Delta Z) \right|^2. \tag{6}$$

Unlike the above cases, the self-imaging is along straight lines regardless of the value of α, and the Airy–Talbot distance becomes

$$Z_T = \frac{2\pi}{|\alpha|Z}. \tag{7}$$

The theoretical analysis can be verified by performing numerical simulations. Figure 4(a) shows the Airy–Talbot carpet for $\alpha = 1$, where the other parameters are the same as in
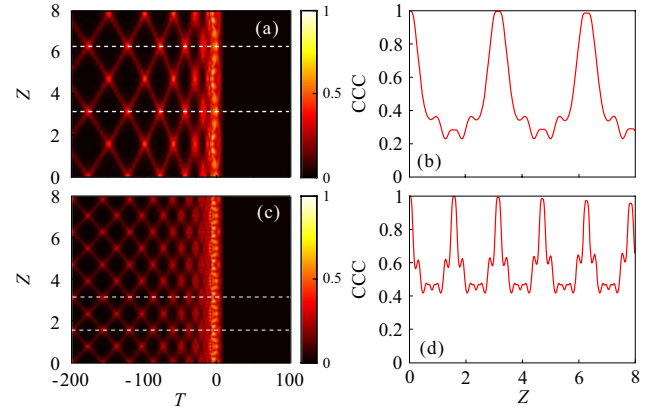

Fig. 4. (a) Temporal evolution of the input composed of stationary Airy pulses with a specific stretch factor of $T_0 = (2\alpha/k)^{1/3}$. Here, we choose $\alpha = 1$, and other parameters are the same as in Fig. 1. (b) Corresponding CCC variation with respect to Z. (c), (d) Same as (a) and (b) but for $\alpha = 2$.

Fig. 1. The self-imaging is along straight lines, and the corresponding Airy–Talbot distance is $Z_T = \pi$. The white dashed lines in Fig. 4(a) denote the first and second self-imaging positions. The self-imaging effect can also be validated through CCC, which varies periodically with Z and reaches $\text{CCC} = 1$ at $Z = mZ_T$ ($m = 1,2,\dots$), as shown in Fig. 4(b). For $\alpha = 2$, the Airy–Talbot distance becomes $Z_T = \pi/2$. The corresponding Airy–Talbot carpet and the CCC evolution with respect to Z are shown in Figs. 4(c) and 4(d), respectively. All results agree well with the theoretical predictions. Note that as $\alpha = -1/2$, Eqs. (5)–(7) are reduced to Eqs. (2)–(4) for $C = 0$, respectively. Thus, the self-imaging shown in Fig. 1(c) is also along straight lines.

Finally, we investigate the Airy–Talbot effect in symmetric linear potentials. The theoretical model can be described by

$$i\frac{\partial U}{\partial Z} + \frac{1}{2}k\frac{\partial^2 U}{\partial T^2} \pm \alpha TU = 0, \tag{8}$$

where we choose "+/−" for $T < 0$ or $T > 0$. The eigensolution of Eq. (8) takes the form of the Airy function[34]

$$U(T,Z) = A\text{Ai}[\mp T_0(T\mp\delta)]\exp(i\alpha\delta Z), \tag{9}$$

where "−(+)" corresponds to $T < 0$ ($T > 0$), respectively. A is an arbitrary amplitude coefficient, and δ characterizes the main-lobe position of each Airy wave packet. Based on the continuity of U and $\mathrm{d}U/\mathrm{d}T$ at $T = 0$, we can obtain the discrete set of values of δ[34]. For an input composed of many Airy pulses with different δ in a symmetric linear potential, the self-imaging effect can be observed when all of the Airy components are in phase during propagation.

Figure 5(a) depicts the temporal profile of an input formed by the superposition of two Airy pulses with $\delta = 2.588$ and 3.882 in the case of $\alpha = -1$. Here, we choose $A = 1$ and $k = 1$. The corresponding Airy–Talbot distance is $Z_T = 4.86$. Figure 5(b) shows the Airy–Talbot carpet in the $T - Z$ plane. The white dashed lines in Fig. 5(b) denote the two positions of $Z = 4.86$
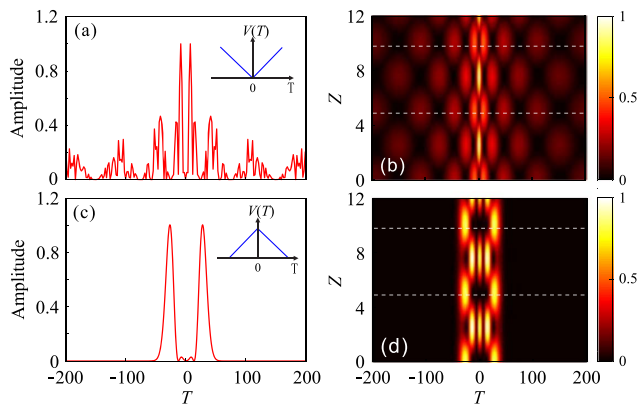
Fig. 5. (a) Temporal waveform of the input composed of two Airy pulses with $\delta = 2.588$ and 3.882 in the case of $\alpha = -1$. (b) Corresponding intensity pattern in the T–Z plane. (c), (d) Same as (a) and (b) but for $\alpha = 1$. Here, we choose $\delta = -2.588$ and -3.882. $A = 1$ and $k = 1$.

and 9.71, at which the self-images are formed. Comparably, for $\alpha = 1$, the Airy–Talbot effect in symmetric linear potential can also be obtained by choosing $\delta = -2.588$ and -3.882. The corresponding temporal waveform of input is plotted in Fig. 5(c). The temporal evolution of input is shown in Fig. 5(d), where the Airy–Talbot distance is the same as that for $\alpha = 1$.

4. Conclusion

In summary, we have studied the Airy–Talbot effects of Airy pulse trains in time-dependent linear potentials. The parabolic space–time trajectory of self-imaging is determined by both the dispersion sign and the linear potential gradient. For the FEAPs, the effect can be observed only in a limited distance. The self-imaging trajectory can also be engineered by imposing linearly time-varying phases on the pulse train. For an input composed of stationary Airy pulses, the self-imaging follows straight lines, and the Airy–Talbot distance can be controlled by varying the linear potential gradient. The study provides a promising way to manipulate the self-imaging of aperiodic optical fields. The extension of the effects to other wave systems, such as Airy plasmons[11], spatial Airy beams[12], and Airy water waves[18], may find great applications in information transportation and reconstruction systems.

References

1. H. F. Talbot, "Facts relating to optical science," Philos. Mag. **9**, 401 (1836).
2. J. Wen, Y. Zhang, and M. Xiao, "The Talbot effect: recent advances in classical optics, nonlinear optics, and quantum optics," Adv. Opt. Photon. **5**, 83 (2013).
3. G. P. Agrawal, *Nonlinear Fiber Optics* (Academic, 2013).
4. J. Azaña and M. A. Muriel, "Temporal Talbot effect in fiber gratings and its applications," Appl. Opt. **38**, 6700 (1999).
5. R. Yang, Z. Xue, Z. Shi, L. Zhou, and L. Zhu, "Scalable Talbot effect of periodic array objects," Chin. Opt. Lett. **18**, 030501 (2020).
6. Y. Lumer, L. Drori, Y. Hazan, and M. Segev, "Accelerating self-imaging: the Airy–Talbot effect," Phys. Rev. Lett. **115**, 013901 (2015).
7. Y. Zhang, H. Zhong, M. R. Belić, X. Liu, W. Zhong, Y. Zhang, and M. Xiao, "Dual accelerating Airy–Talbot recurrence effect," Opt. Lett. **40**, 5742 (2015).
8. Y. Zhang, H. Zhong, M. R. Belić, C. Li, Z. Zhang, F. Wen, Y. Zhang, and M. Xiao, "Fractional nonparaxial accelerating Talbot effect," Opt. Lett. **41**, 3273 (2016).
9. G. A. Siviloglou and D. N. Christodoulides, "Accelerating finite energy Airy beams," Opt. Lett. **32**, 979 (2007).
10. G. A. Siviloglou, J. Broky, A. Dogariu, and D. N. Christodoulides, "Observation of Accelerating Airy beams," Phys. Rev. Lett. **99**, 213901 (2007).
11. W. Liu, D. N. Neshev, I. V. Shadrivov, A. E. Miroshnichenko, and Y. S. Kivshar, "Plasmonic Airy beam manipulation in linear optical linears," Opt. Lett. **36**, 1164 (2011).
12. Z. Ye, S. Liu, C. Lou, P. Zhang, Y. Hu, D. Song, J. Zhao, and Z. Chen, "Acceleration control of Airy beams with optically induced refractive-index gradient," Opt. Lett. **36**, 3230 (2011).
13. X. Huang, Z. Deng, and X. Fu, "Dynamics of finite energy Airy beams modeled by the fractional Schrödinger equation with a linear potential," J. Opt. Soc. Am. B **34**, 3044 (2017).
14. S. Jia, J. Lee, and J. W. Fleischer, "Diffusion-trapped Airy beams in photorefractive media," Phys. Rev. Lett. **104**, 253904 (2010).
15. N. K. Efremids, "Airy trajectory engineering in dynamic linear index potentials," Opt. Lett. **36**, 3006 (2011).
16. C.-Y. Hwang, K.-Y. Kim, and B. Lee, "Dynamic control of circular Airy beams with linear optical potentials," IEEE Photon. J. **4**, 174 (2012).
17. H. Zhong, Y. Zhang, M. R. Belié, C. Li, F. Wen, Z. Zhang, and Y. Zhang, "Controllable circular Airy beams via dynamic linear potential," Opt. Express **24**, 7495 (2016).
18. G. G. Rozenman, M. Zimmermann, M. A. Efremov, W. P. Schleich, L. Shemer, and A. Arie, "Amplitude and phase of wave packets in a linear potential," Phys. Rev. Lett. **122**, 124302 (2019).
19. X. Yan, L. Guo, M. Cheng, and S. Chai, "Free-space propagation of autofocusing Airy vortex beams with controllable intensity gradients," Chin. Opt. Lett. **17**, 040101 (2019).
20. Y. Zhang, B. Wei, S. Liu, P. Li, X. Chen, Y. Wu, X. Dou, and J. Zhao, "Circular Airy beams realized via the photopatterning of liquid crystals," Chin. Opt. Lett. **18**, 080008 (2020).
21. K. Zhan, Z. Yang, and B. Liu, "Trajectory engineering of Airy–Talbot effect via dynamic linear potential," J. Opt. Soc. Am. B **35**, 3044 (2018).
22. K. Zhan, J. Wang, R. Jiao, Z. Yang, and B. Liu, "Self-imaging effect based on circular Airy beams," Ann. Phys. **531**, 1900293 (2019).
23. K. Zhan, R. Jiao, J. Wang, W. Zhang, Z. Yang, and B. Liu, "Self-imaging effect based on Airy beams with quadratic phase modulation," Ann. Phys. **532**, 1900546 (2020).
24. Z. Li, P. Zhang, X. Mu, P. Jia, Y. Hu, Z. Chen, and J. Xu, "Guiding and routing of a weak signal via a reconfigurable gravity-like potential," Photon. Res. **7**, 1087 (2019).
25. P. Jia, Z. Li, Y. Hu, Z. Chen, and J. Xu, "Visualizing a nonlinear response in a Schrödinger wave," Phys. Rev. Lett. **123**, 234101 (2019).
26. I. Kaminer, Y. Lumer, M. Segev, and D. N. Christodoulides, "Causality effects on accelerating light pulses," Opt. Express **19**, 23132 (2011).
27. T. Han, B. Wang, and P. Lu, "Accelerating self-imaging effect for Airy pulse trains," Phys. Rev. A **99**, 053807 (2019).
28. M. Miyagi and S. Nishida, "Pulse spreading in a single-mode fiber due to third-order dispersion," Appl. Opt. **18**, 678 (1979).
29. C. Ament, P. Polynkin, and J. V. Moloney, "Supercontinuum generation with femtosecond self-healing Airy pulses," Phys. Rev. Lett. **107**, 243901 (2011).
30. C.-C. Chang, H. P. Sardesai, and A. M. Weiner, "Dispersion-free fiber transmission for femtosecond pulses by use of a dispersion-compensating fiber and a programmable pulse shaper," Opt. Lett. **23**, 283 (1998).

31. T. Han, H. Chen, C. Qin, W. Li, B. Wang, and P. Lu, "Airy pulse shaping using time-dependent power-law potentials," Phys. Rev. A **97**, 063815 (2018).

32. A. Banerjee and S. Roy, "Trajectory manipulation of an Airy pulse near zero-dispersion wavelength under a free-carrier-generated linear potential," Phys. Rev. A **100**, 053816 (2019).

33. S. Wang, D. Fan, X. Bai, and X. Zeng, "Propagation dynamics of Airy pulses in optical fibers with periodic dispersion modulation," Phys. Rev. A **89**, 023802 (2014).

34. N. K. Efremidis, D. G. Papazoglou, and S. Tzortzakis, "Linear and nonlinear waves in surface and wedge index potentials," Opt. Lett. **37**, 1874 (2012).

QUERY

1: AU: Are edits to the title okay?

Yes, it is OK.